

# NONCONFORMING FINITE ELEMENTS FOR REISSNER-MINDLIN PLATES

C. CHINOSI

*Dipartimento di Scienze e Tecnologie Avanzate,  
Università del Piemonte Orientale,  
Via Bellini 25/G, 15100 Alessandria, Italy  
E-mail: chinosi@mfn.unipmn.it*

C. LOVADINA AND L.D. MARINI

*Dipartimento di Matematica, Università di Pavia,  
and IMATI-CNR,  
Via Ferrata 1, 27100 Pavia, Italy  
E-mails: carlo.lovadina@unipv.it , marini@imati.cnr.it*

We report on recent results about some nonconforming finite elements for plates, introduced and analyzed in [6], [12] and [9]. All the elements are locking-free and exhibit optimal convergence rates.

## Introduction

As it is well-known (cf. [4], for instance), the numerical treatment of the Reissner-Mindlin model requires special care, in order to avoid the so-called *shear locking phenomenon* and the occurrence of *spurious modes*.

The *shear locking* has its roots from the shear energy term, which for “small” thickness enforces the *Kirchhoff* constraint. It turns out that for simple low-order elements this constraint is generally too severe, thus compromising the quality of the obtained discrete solution. A general and commonly adopted strategy to overcome the problem consists in modifying, at the discrete level, the shear energy term, with the aim of reducing its influence. In most cases the modification can be interpreted as the result of (or directly arises from) a mixed approach to the problem.

However, a careless choice of the shear reduction procedure may cause a loss of stability, typically enlightened by the presence of undesirable oscillating components in the discrete solution (the *spurious modes*).

We point out that nowadays a wide choice of good elements are available

in the literature (see, for instance, [1]–[3], [5]–[7], [11]–[15], and the references therein).

The aim of this Note is to discuss some finite element schemes recently proposed and studied in [6], [9], and [12]. These elements are all based on a mixed *nonconforming approach*, and they have some features which seem to be favorable for a possible extension to the more complex (and more interesting) case of shell problems. Indeed, the methods we will consider take advantage of *low-order* polynomial approximations; they are locking-free and optimally convergent; finally, once the mixed variables (i.e. the shear stresses) have been eliminated, all the remaining unknowns (i.e. rotations and deflections) *share the same nodes and degrees of freedom*.

The paper is organized as follows. In Section 1 we recall the Reissner-Mindlin equations, and we briefly present the elements of [6] and [12]. Section 2 is devoted to numerical results.

### 1. The Reissner-Mindlin problem and the nonconforming elements

The Reissner-Mindlin equations for a clamped plate require to find  $(\boldsymbol{\theta}, w, \boldsymbol{\gamma})$  such that

$$-\operatorname{div} \mathbf{C} \boldsymbol{\varepsilon}(\boldsymbol{\theta}) - \boldsymbol{\gamma} = 0 \quad \text{in } \Omega, \quad (1)$$

$$-\operatorname{div} \boldsymbol{\gamma} = g \quad \text{in } \Omega, \quad (2)$$

$$\boldsymbol{\gamma} = \lambda t^{-2}(\boldsymbol{\nabla} w - \boldsymbol{\theta}) \quad \text{in } \Omega, \quad (3)$$

$$\boldsymbol{\theta} = 0, \quad w = 0 \quad \text{on } \partial\Omega. \quad (4)$$

In (1)–(3),  $\Omega$  is the midplane, regular and bounded,  $t$  is the thickness,  $\mathbf{C}$  is the tensor of bending moduli, and  $\lambda$  is the shear modulus (incorporating also the shear correction factor). Moreover,  $\boldsymbol{\theta}$  represents the rotations,  $w$  the transversal displacement,  $\boldsymbol{\gamma}$  the scaled shear stresses and  $g$  a given transversal load. Finally,  $\boldsymbol{\varepsilon}$  is the usual symmetric gradient operator. The classical variational formulation of problem (1)–(4) is

$$\left\{ \begin{array}{ll} \text{Find } (\boldsymbol{\theta}, w, \boldsymbol{\gamma}) \in \mathbf{H}_0^1(\Omega) \times H_0^1(\Omega) \times \mathbf{L}^2(\Omega) : & \\ a(\boldsymbol{\theta}, \boldsymbol{\eta}) + (\boldsymbol{\nabla} w - \boldsymbol{\eta}, \boldsymbol{\gamma}) = (g, v) & (\boldsymbol{\eta}, v) \in \mathbf{H}_0^1(\Omega) \times H_0^1(\Omega), \\ (\boldsymbol{\nabla} w - \boldsymbol{\theta}, \boldsymbol{\tau}) - \lambda^{-1} t^2 (\boldsymbol{\gamma}, \boldsymbol{\tau}) = 0 & \boldsymbol{\tau} \in \mathbf{L}^2(\Omega), \end{array} \right. \quad (5)$$

where  $(\cdot, \cdot)$  is the inner-product in  $L^2(\Omega)$  (or in  $\mathbf{L}^2(\Omega)$ ), and

$$a(\boldsymbol{\theta}, \boldsymbol{\eta}) := \int_{\Omega} \mathbf{C} \boldsymbol{\varepsilon}(\boldsymbol{\theta}) : \boldsymbol{\varepsilon}(\boldsymbol{\eta}) \, dx. \quad (6)$$

We now introduce nonconforming finite element approximations of problem (1)–(4) using the approach detailed in [6]. Let then  $\mathcal{T}_h$  be a regular decomposition of  $\Omega$  into triangular elements  $T$  (see [10], for example), and let us set  $H^1(\mathcal{T}_h) := \prod_{T \in \mathcal{T}_h} H^1(T)$ . Following [1], we define suitable jump operators. Let  $\mathcal{E}_h$  denote the set of all the edges in  $\mathcal{T}_h$ , and  $\mathcal{E}_h^{\text{in}}$  the set of internal edges. Let  $e$  be an internal edge of  $\mathcal{T}_h$ , shared by two elements  $T^+$  and  $T^-$ , and let  $\varphi$  denote a function in  $H^1(\mathcal{T}_h)$ , or a vector in  $\mathbf{H}^1(\mathcal{T}_h)$ . For a scalar function  $\varphi \in H^1(\mathcal{T}_h)$  we define its jump as

$$[\varphi] = \varphi^+ \mathbf{n}^+ + \varphi^- \mathbf{n}^- \quad \forall e \in \mathcal{E}_h^{\text{in}}, \quad (7)$$

while the jump of a vector  $\boldsymbol{\varphi} \in \mathbf{H}^1(\mathcal{T}_h)$  is given by

$$[\boldsymbol{\varphi}] = (\boldsymbol{\varphi}^+ \otimes \mathbf{n}^+)_S + (\boldsymbol{\varphi}^- \otimes \mathbf{n}^-)_S \quad \forall e \in \mathcal{E}_h^{\text{in}}, \quad (8)$$

where  $(\boldsymbol{\varphi} \otimes \mathbf{n})_S$  denotes the symmetric part of the tensor product, and  $\mathbf{n}^+$  (resp.  $\mathbf{n}^-$ ) is the outward unit normal to  $\partial T^+$  (resp. to  $\partial T^-$ ). On the boundary edges we define jumps of scalars as  $[\varphi] = \varphi \mathbf{n}$ , and jumps of vectors as  $[\boldsymbol{\varphi}] = (\boldsymbol{\varphi} \otimes \mathbf{n})_S$ , where  $\mathbf{n}$  is the outward unit normal to  $\partial\Omega$ . Following the ideas of [6], we now select finite element spaces  $\boldsymbol{\Theta}_h \subset \mathbf{H}^1(\mathcal{T}_h)$ ,  $W_h \subset H^1(\mathcal{T}_h)$ , and  $\boldsymbol{\Gamma}_h \subset \mathbf{L}^2(\Omega)$ , with the property:  $\boldsymbol{\nabla}_h W_h \subseteq \boldsymbol{\Gamma}_h$ , where  $\boldsymbol{\nabla}_h$  denotes the gradient operator element by element. The discrete problem is then

$$\begin{cases} \text{Find } (\boldsymbol{\theta}_h, w_h, \boldsymbol{\gamma}_h) \in \boldsymbol{\Theta}_h \times W_h \times \boldsymbol{\Gamma}_h : \\ a_h(\boldsymbol{\theta}_h, \boldsymbol{\eta}_h) + (\boldsymbol{\gamma}_h, \boldsymbol{\nabla}_h w_h - \mathbf{R}_h \boldsymbol{\eta}_h) = (g, w_h) & (\boldsymbol{\eta}_h, w_h) \in \boldsymbol{\Theta}_h \times W_h, \\ (\boldsymbol{\nabla}_h w_h - \mathbf{R}_h \boldsymbol{\theta}_h, \boldsymbol{\tau}_h) - \lambda^{-1} t^2 (\boldsymbol{\gamma}_h, \boldsymbol{\tau}_h) = 0 & \boldsymbol{\tau}_h \in \boldsymbol{\Gamma}_h. \end{cases} \quad (9)$$

Above, the bilinear form  $a_h(\cdot, \cdot)$  is defined, for piecewise regular functions, by

$$a_h(\boldsymbol{\theta}, \boldsymbol{\eta}) := \sum_{T \in \mathcal{T}_h} \int_T \mathbf{C} \boldsymbol{\varepsilon}(\boldsymbol{\theta}) : \boldsymbol{\varepsilon}(\boldsymbol{\eta}) \, dx + p_{\boldsymbol{\Theta}}(\boldsymbol{\theta}, \boldsymbol{\eta}), \quad (10)$$

where  $p_{\boldsymbol{\Theta}}$  is a penalty term given by

$$p_{\boldsymbol{\Theta}}(\boldsymbol{\theta}, \boldsymbol{\eta}) := \sum_{e \in \mathcal{E}_h} \frac{\kappa_e}{|e|} \int_e [\boldsymbol{\theta}] : [\boldsymbol{\eta}] \, ds \quad (|e| := \text{length of the edge } e), \quad (11)$$



- The reduction operator  $\mathbf{R}_h : \mathbf{H}^1(\mathcal{T}_h) \rightarrow \mathbf{\Gamma}_h$  is defined locally by:

$$\int_T (\boldsymbol{\eta} - \mathbf{R}_h \boldsymbol{\eta}) dx = 0 \quad \forall T \in \mathcal{T}_h, \quad \boldsymbol{\eta} \in \mathbf{H}^1(\mathcal{T}_h), \quad (18)$$

$$\int_T \operatorname{div}(\boldsymbol{\eta} - \mathbf{R}_h \boldsymbol{\eta}) dx = 0 \quad \forall T \in \mathcal{T}_h, \quad \boldsymbol{\eta} \in \mathbf{H}^1(\mathcal{T}_h). \quad (19)$$

### 1.2. The “conforming bubble” element

This element is also mentioned in [6], and it differs from the previous one only for the choice of the type of bubble. Define, on a generic triangle  $T \in \mathcal{T}_h$ :

$$B_3(T) := \operatorname{Span} \{b_3\}, \quad (20)$$

where  $b_3$  denotes the standard cubic bubble. In barycentric coordinates its expression is, for instance,

$$b_3 = 27\lambda_1\lambda_2\lambda_3. \quad (21)$$

This scheme is characterized by the following choices.

- The finite element spaces are

$$\Theta_h = \{\boldsymbol{\eta} : \boldsymbol{\eta}|_T \in (P_1(T) \oplus B_3(T))^2, \int_e [\boldsymbol{\eta}] ds = 0 \quad \forall e \in \mathcal{E}_h\}, \quad (22)$$

$$W_h = \{v : v|_T \in P_1(T) \oplus B_3(T), \int_e [v] ds = 0 \quad \forall e \in \mathcal{E}_h\}, \quad (23)$$

$$\mathbf{\Gamma}_h = \{\boldsymbol{\tau} : \boldsymbol{\tau}|_T \in P_0(T)^2 \oplus \nabla B_3(T)\}. \quad (24)$$

- The reduction operator  $\mathbf{R}_h : \mathbf{H}^1(\mathcal{T}_h) \rightarrow \mathbf{\Gamma}_h$  is the same defined in (18)-(19).

### 1.3. The $P_1^{NC} - P_1^{NC} - P_0$ element

This element has been introduced and analyzed in [12], and it is characterized by the following choices.

- The finite element spaces are

$$\Theta_h = \{\boldsymbol{\eta} : \boldsymbol{\eta}|_T \in (P_1(T))^2, \int_e [\boldsymbol{\eta}] ds = 0 \quad \forall e \in \mathcal{E}_h\}, \quad (25)$$

$$W_h = \{v : v|_T \in P_1(T), \int_e [v] ds = 0 \quad \forall e \in \mathcal{E}_h\}, \quad (26)$$

$$\mathbf{\Gamma}_h = \{\boldsymbol{\tau} : \boldsymbol{\tau}|_T \in (P_0(T))^2\}. \quad (27)$$

•  $\mathbf{R}_h$  is simply the  $L^2$ -projection operator onto the piecewise constant functions (see (18)).

All the elements presented in Sections 1.1–1.3 are first order convergent for the kinematic variables. More precisely, for each method it holds (see [6] and [12])

$$\|\boldsymbol{\theta} - \boldsymbol{\theta}_h\|_{1,h} + \|w - w_h\|_{1,h} \leq Ch, \quad (28)$$

where  $\|\cdot\|_{1,h}$  denotes the  $H^1$ -broken norm. Furthermore, it has been proved in [9] that for the element of Section 1.3 one has the  $L^2$  bounds:

$$\|\boldsymbol{\theta} - \boldsymbol{\theta}_h\|_0 + \|w - w_h\|_0 \leq Ch^2. \quad (29)$$

## 2. Numerical results

In this section we present some numerical results showing the behavior of the nonconforming elements of Sections 1.1–1.3. For comparison purposes, we consider also the stable and first order convergent Arnold-Falk element, proposed and analyzed in [2]. As a test problem we take an isotropic and homogeneous plate  $\Omega = (0, 1) \times (0, 1)$ , clamped on the whole boundary, for which the analytical solution is explicitly known (see [8] or [9] for all the details). We analyze the convergence properties of the elements by considering different uniform decompositions as shown in Figure 1(left) with  $h = 1/4, 1/8, 1/16, 1/32$ , and keeping the thickness sufficiently small ( $t = .001$ ). Moreover, in the penalty term (11) we set  $\kappa_e = |\mathbf{C}| \simeq$  euclidean norm of  $\mathbf{C}$ .

In Figures 2 and 3 we report the relative errors, in the  $L^2$ -norm, for rotations and deflection respectively.

Instead, Figures 4 and 5 show the relative errors for rotations and deflection, respectively, in the energy norm.

We conclude this Note by briefly commenting on the effect of choosing a “too small” penalty parameters  $\kappa_e$  in (11) (cf. Remark 1.2). To this aim, we consider the same test problem as before, but we use the mesh shown in Figure 1(right). Figures 6–7 display the profiles of the analytical solution for the first component of the rotation vector  $\theta_1$ , and for the deflection  $w$ , respectively. Figures 8–9 show the profiles of the corresponding discrete solutions, obtained by the element of Section 1.3 with the *reasonable* choice  $\kappa_e = |\mathbf{C}|$ ; we may observe that the profiles are quite accurately captured. Figures 10–11 show the profiles of the discrete solutions, this time with the *wrong* choice  $\kappa_e = |\mathbf{C}| \cdot 10^{-5}$ ; undesirable oscillations clearly appear on the approximation of both the rotations and the vertical displacements.

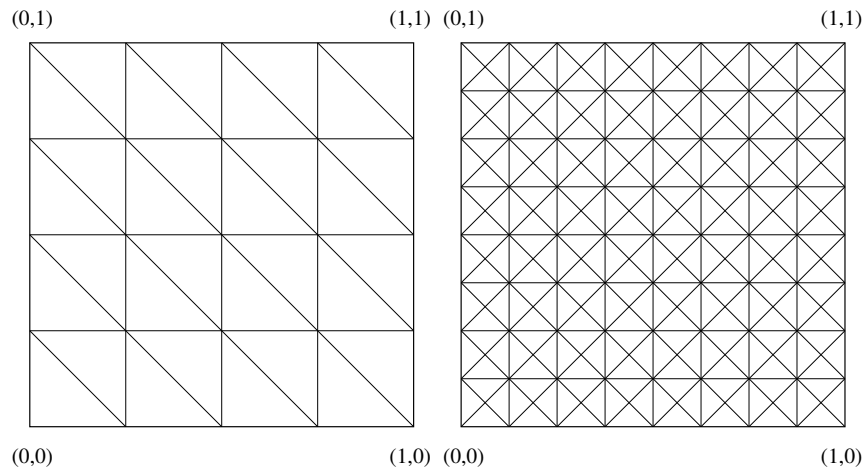
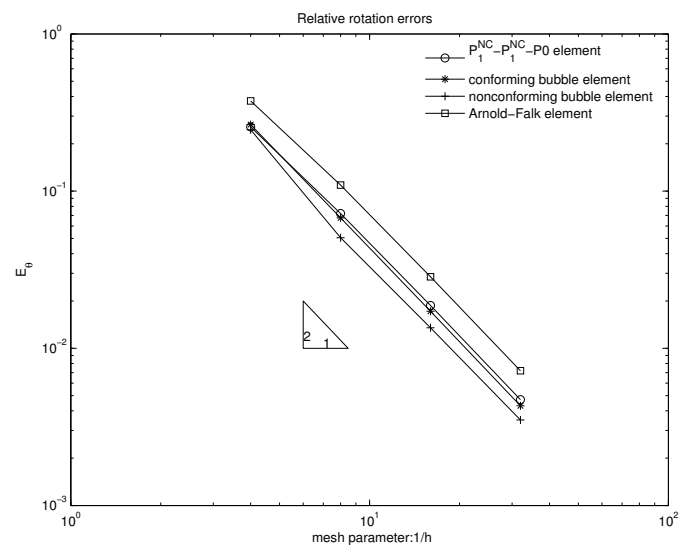


Figure 1. Adopted meshes.

Figure 2. Relative rotation errors in  $L^2$ -norm versus  $1/h$ .

## References

1. D.N. Arnold, F. Brezzi and L.D. Marini, A family of discontinuous Galerkin finite elements for the Reissner-Mindlin plate, *J. Sci. Comp.* (to appear).
2. D.N. Arnold and R.S. Falk, A uniformly accurate finite element method for

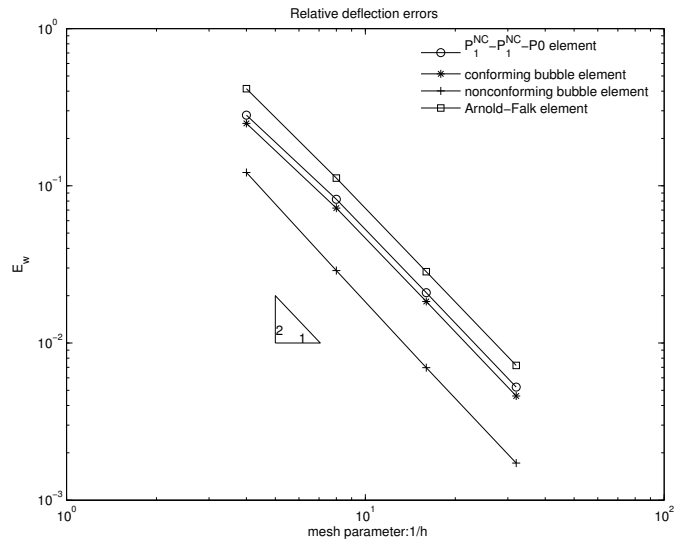


Figure 3. Relative deflection errors in  $L^2$ -norm versus  $1/h$ .

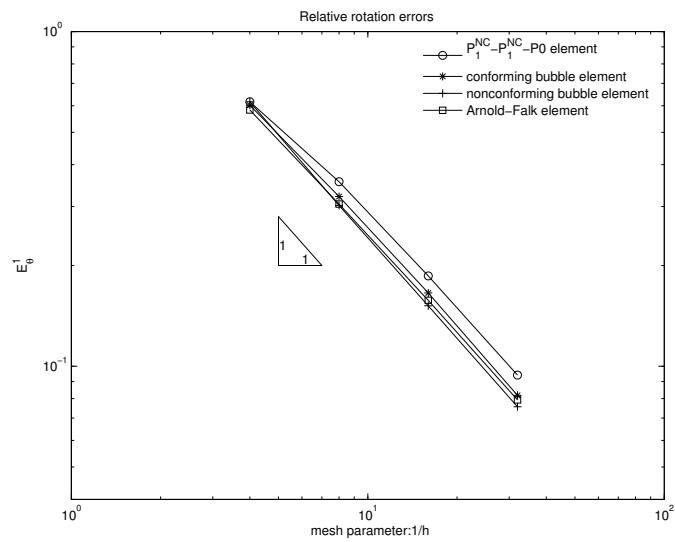


Figure 4. Relative rotation errors in the energy norm versus  $1/h$ .

the Reissner-Mindlin plate, *SIAM J. Numer. Anal.* **26**, 1276–1290 (1989).

3. F. Auricchio and C. Lovadina, Analysis of kinematic linked interpolation meth-

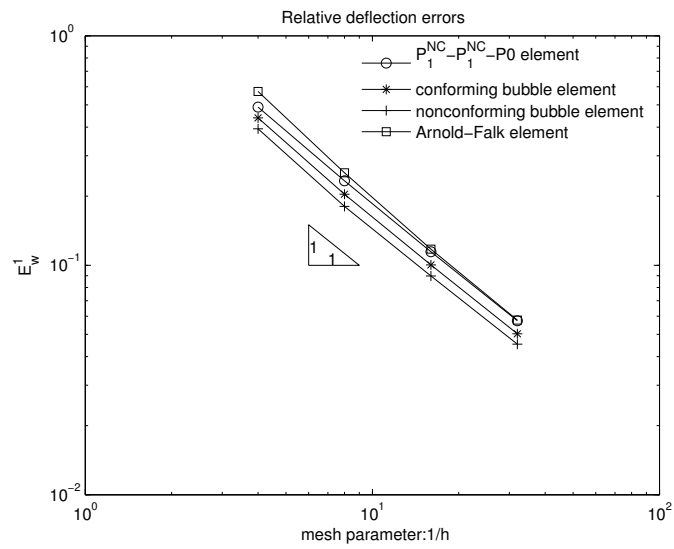


Figure 5. Relative deflection errors in the energy norm versus  $1/h$ .

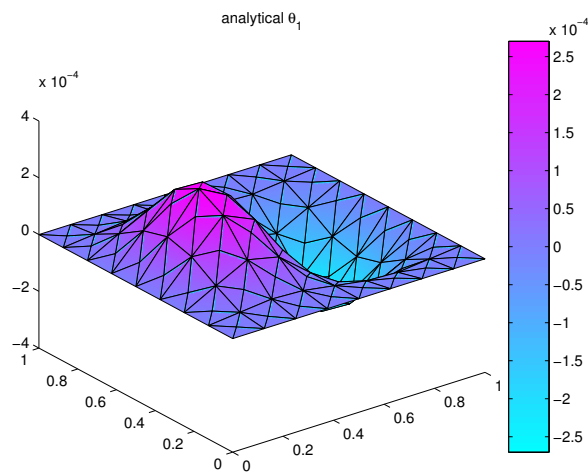
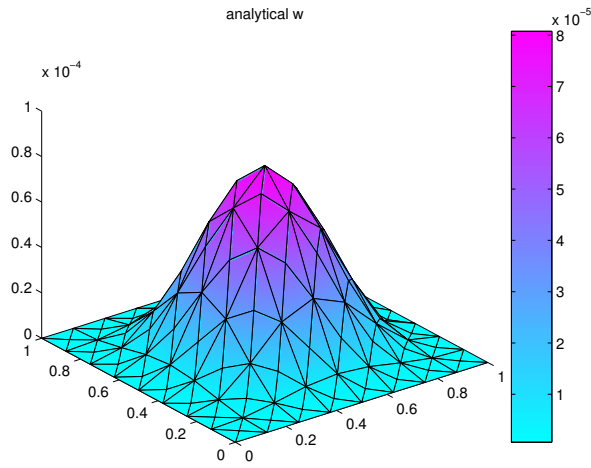
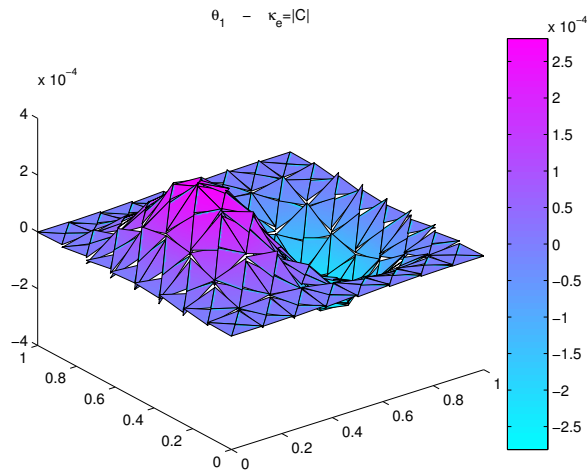


Figure 6. Profile of the analytical solution  $\theta_1$ .

- ods for Reissner-Mindlin plate problems, *Comput. Methods Appl. Mech. Engrg.* **190**, 2465–2482 (2001).
4. F. Brezzi and M. Fortin, *Mixed and Hybrid Finite Element Methods*, Springer

Figure 7. Profile of the analytical solution  $w$ .Figure 8. Profile of the approximation to  $\theta_1$  with  $\kappa_e = |C|$ .

Verlag, 1991.

5. F. Brezzi, M. Fortin and R. Stenberg, Error analysis of mixed-interpolated elements for Reissner-Mindlin plates, *Math. Models Methods Appl. Sci.* **1**, 125–151 (1991).

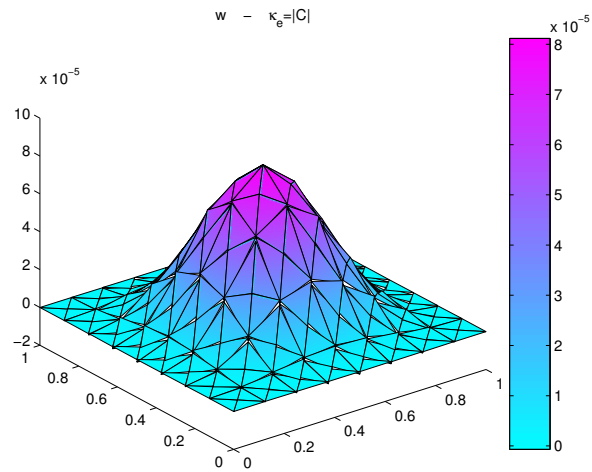


Figure 9. Profile of the approximation to  $w$  with  $\kappa_e = |C|$ .

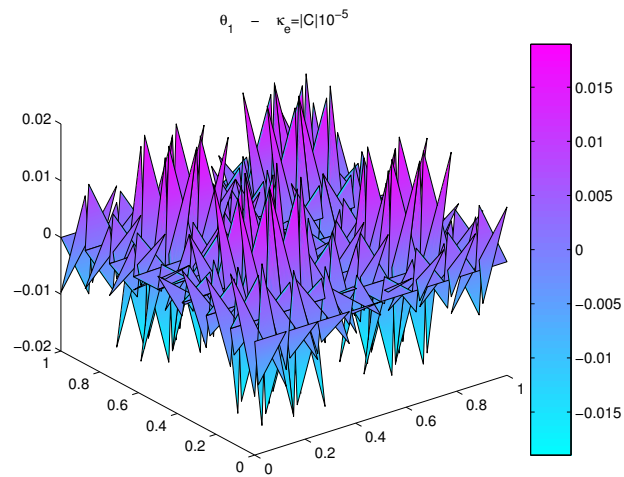


Figure 10. Profile of the approximation to  $\theta_1$  with  $\kappa_e = |C| \cdot 10^{-5}$ .

6. F. Brezzi and L.D. Marini, A nonconforming element for the Reissner-Mindlin plate, *Computers & Structures* **81**, 515–522 (2003).
7. D. Chapelle and R. Stenberg, An optimal low-order locking-free finite element method for Reissner-Mindlin plates, *Math. Models and Methods in Appl. Sci.*

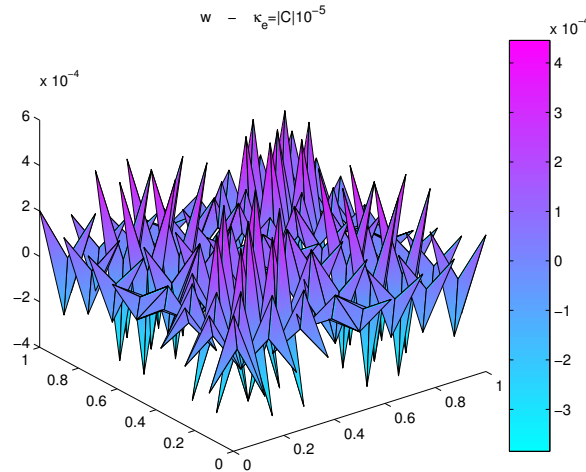


Figure 11. Profile of the approximation to  $w$  with  $\kappa_e = |\mathbf{C}| \cdot 10^{-5}$ .

- 8, 407–430 (1998).
8. C. Chinosi and C. Lovadina, Numerical analysis of some mixed finite element methods for Reissner-Mindlin plates, *Comput. Mechanics* **16**, 36–44 (1995).
  9. C. Chinosi, C. Lovadina and L.D. Marini, Nonconforming locking-free finite elements for Reissner-Mindlin plates, submitted to *Comput. Methods Appl. Mech. Engrg.*.
  10. P.G. Ciarlet, *The Finite Element Method for Elliptic Problems*, North-Holland, 1978.
  11. R.S. Falk and T. Tu, Locking-free finite elements for the Reissner-Mindlin plate, *Math. Comp.* **69**, 911–928 (2000).
  12. C. Lovadina, A low-order nonconforming finite element for Reissner-Mindlin plates, *SIAM J. Numer. Anal.* (to appear).
  13. R. Stenberg, A new finite element formulation for the plate bending problem, in **Asymptotic Methods for Elastic Structures**, eds. P.G. Ciarlet, L. Trabucho and J. Viaño, Walter de Gruyter & Co., 209–221 (1995).
  14. R.L. Taylor and F. Auricchio, Linked interpolation for Reissner-Mindlin plate elements: Part II– A simple triangle, *Int. J. Numer. Methods Eng.* **36**, 3057–3066 (1993).
  15. A. Tessler and T.J.R. Hughes, A three-node Mindlin plate element with improved transverse shear, *Comput. Methods Appl. Mech. Engrg.* **50**, 71–101 (1985).